AFRL-AFOSR-UK-TR-2017-0028

Radiative transport modeling of thermal barrier coatings

Bauke Heeg
Lumium

03/24/2017
Final Report

Air Force Research Laboratory
AF Office Of Scientific Research (AFOSR)/ IOE
Arlington, Virginia 22203
Air Force Materiel Command

REPORT DOCUMENTATION PAGE

Form Approved
OMB No. 0704-0188

1. REPORT DATE *(DD-MM-YYYY)*	2. REPORT TYPE	3. DATES COVERED *(From - To)*
24-03-2017	Interim Progress Report #1	March 2016 – February 2017

4. TITLE AND SUBTITLE

Radiative Transport Modelling of Thermal Barrier Coatings

5a. CONTRACT NUMBER
FA9550-16-C-0006

5b. GRANT NUMBER

5c. PROGRAM ELEMENT NUMBER

6. AUTHOR(S)

Heeg, Bauke, Dr.

5d. PROJECT NUMBER

5e. TASK NUMBER

5f. WORK UNIT NUMBER

7. PERFORMING ORGANIZATION NAME(S) AND ADDRESS(ES)

Lumium *optical precision measurement solutions*
Eewal 84
8911 GV Leeuwarden, The Netherlands

8. PERFORMING ORGANIZATION REPORT NUMBER
PRAF1.doc

9. SPONSORING/MONITORING AGENCY NAME(S) AND ADDRESS(ES)

European Office of Aerospace Research and Development (EOARD)
86 Blenheim Crescent
Ruislip Middlesex HA47HB
United Kingdom

10. SPONSOR/MONITOR'S ACRONYM(S)

11. SPONSOR/MONITOR'S REPORT NUMBER(S)

12. DISTRIBUTION/AVAILABILITY STATEMENT

13. SUPPLEMENTARY NOTES

14. ABSTRACT

The aim of this project is to develop an accurate analytical model of radiative transfer through porous ceramic thermal barrier coatings (TBCs). In particular, the model is aimed at computation of the integrated optical path-length as a function of several basic parameters including bulk scatter and absorption coefficients. Further, the model will need to take into account the effects of interface reflections and a multilayer structure. Such a model is of interest for use in low coherence interferometry measurements (also referred to as optical coherence tomography) on TBCs, in particular those that have been infiltrated with molten silicates (CMAS – calcium, magnesium, aluminum oxide silicates).

15. SUBJECT TERMS

16. SECURITY CLASSIFICATION OF:			17. LIMITATION OF ABSTRACT	18. NUMBER OF PAGES	19a. NAME OF RESPONSIBLE PERSON
a. REPORT	b. ABSTRACT	c. THIS PAGE			Dr. Bauke Heeg
Unclassified	Unclassified	Unclassified	SAR	15	19b. TELEPHONE NUMBER *(Include area code)* +31 58 8431 782

Standard Form 298 (Rev. 8/98)

INTRODUCTION

This project focuses on a general problem encountered in the application of low coherence interferometry (LCI, also referred to as Optical Coherence Tomography, OCT) to measure the fundamental optical properties of scattering materials, in the present case of porous ceramic TBCs and other materials used in extreme environments: namely, that currently available theoretical models describe experimental data inadequately and that better models are needed. This problem is in part application-driven, namely based on the need to be able to extract the radiative properties from the shape the LCI signal. On the other hand, the solution to this problem also has a broader value, since it enables more accurate computation of the radiative heat transfer through TBCs and other materials used in extreme environments.

Objectives

1. The main objective is to develop an analytical model of radiative transfer through porous ceramic thermal barrier coatings. The model to be developed should compute the integrated optical path-length as a function of several basic parameters including bulk scatter and absorption, and takes into account a multilayer structure and interface reflections.
2. The second objective is to validate the analytical model with random number simulations under a variety of conditions, including coating thickness, scatter and absorption parameter values and interface effects.
3. The third objective is to demonstrate that relevant TBC parameters can be measured with LCI, by applying the model to experimental LCI data obtained on a range of test materials.

Change in Objectives: none

Status of Effort

As of the date of this report,

1. A refined random walk simulation code (in two languages) has been finished and tested
2. A new model has been derived with which the integrated pathlength can be computed of photons traveling through an isotropically scattering medium.
3. This new model was tested with the random walk model.

As of to date the project completion is as shown in the following Table.

Table 1: project status summary

Task	Description	Completion (%)	Anticipated completion
1	Review the currently available theoretical models	100	N/A
2	Develop a new radiative transport model	75	June 2017
3	Apply random walk model to test model approaches	75	June 2017
4	Apply the theory to experimental data on TBCs	20	June 2017
5	Report on results and future recommendations	50	July 2017

Project completion is considered to be overall well over 50% from a technical point of view. At least 400 hours have been dedicated to the project, to which a total of 400 hours were assigned in the contract. For this period, 280 hours will be billed to the contract.

DETAILED DESCRIPTION OF WORK PERFORMED DURING THIS REPORT PERIOD

Task 1. Review the currently available theoretical models

The OCT signal typically decays as a function of L, the coherence path-matching separation between signal and reference beam photons. This difference in path length (traveled by signal and reference beam photons) is the result of signal photons travelling a distance L through the sample. Since this distance L is related to scatter and absorption properties of the material, the measured decay function contains precise information on the optical properties of the material under inspection, which is the purpose of OCT measurement. The available models to date do not with sufficient accuracy describe measured OCT signals of even relatively simple systems. For more complex systems, such as TBCs that are partially infiltrated with CMAS, current models fall short of being able to extract useful data. To account for this deficiency, the purpose of this project is to improve models for use in OCT measurements on TBCs.

At the start of the project, the main model approaches identified were

1. Diffusion theory for highly scattering media, see ref. [1]
2. Makino 4-flux type models, see ref. [2]
3. Kubelka-Munk flux model, see ref. [3]
4. Scallan flux model, see ref. [4]
5. Fresnel-Huygens derived theory, ref. [5]

Two of the models, #1 and #5, specifically contain a parameter that is needed in the LCI measurements, namely the integrated pathlength, while the other approaches do not. In this Task, it was investigated how well these two models describe simulation and real data, and which modifications might be needed to further improve them. This comparison between analytical models was made for a significantly simplified system, being that of a semi-infinite, isotropically and purely scattering medium; i.e. effects due to absorption, interface reflections, anisotropy, and multilayer were not included. The underlying thought is that if the model cannot describe this simplified case well, it may not be adequate for more complex structures either.

First, the diffusion theory by Popescu and Dogariu[1] has as the central equation describing the energy flux of the diffusively scattered photons with integrated pathlength L (in their publication called s) as

$$J(L) = (4\pi l_t/3)^{-3/2} z_0 \nu L^{-5/2} \exp\left(\frac{-3{z_0}^2}{4Ll_t}\right), \qquad (1)$$

where l_t is the mean free path, z_0 is a so-called extrapolation length that carries information on the effective reflectivity at the boundaries, and ν is the average transport velocity. It is noted that $J(L)$is not the same as the probability density $P(L)$ of optical path lengths through the medium. Unfortunately, upon consultation of various publications by the authors, it is not entirely clear how the above equation was derived, nor how $J(L)$ relates to $P(L)$. It appears that the above theory is obtained by work from Patterson *et al*,[6] and from various textbooks. Furthermore, it is claimed that the above equation describes measured data well, however we found that the equation is in fact not entirely adequate for both experimental and simulation data. For brevity, the above model is not discussed in detail.

The second model that was investigated is the model derived by Thrane *et al* from Fresnel-Huygens diffraction theory.[5] The Thrane model defines the normalized signal current as a function of integrated pathlength L (in their publication reffered to as z) as

$$\frac{\langle i^2(L)\rangle}{\langle i^2\rangle_0} = \exp(-2\mu_s L) + \frac{4\exp(-\mu_s L)[1-\exp(-\mu_s L)]}{1+w_s^2/w_H^2} + [1-\exp(-\mu_s L)]^2 \frac{w_H^2}{w_s^2}, \qquad (2)$$

where μ_s is the scatter coefficient (in units inverse length) and w_s and w_H are optical parameters. Analysis of the Trane model indicates that it does not account sufficiently for the strongly non-exponential dependence of signal with integrated pathlength, found both in simulation and experimental data. It appears that while the model was derived to account for both single and multiple scattering, it is more strongly favouring single scattering than is witnessed from data.

Originally, and as outlined in the proposal, the analysis of these currently available models was considered to be sufficient to lead to an improved model. The original plan was to select a currently available model and find the modifications needed to better describe both simulated and measured data.

Since thorough analysis of the above models did not lead to either model describing simulated and experimental data adequately, and it was not clear which improvements needed to be made to make theory and data agree better, it was decided to derive a new model from first principles. This effort was in part motivated by the fact that multiple scattering should be well described by Poisson statistics, and that such statistical processes can be well tested with random number simulations.

It is noted that therefore the original Task 2 description, **Modify currently available models**, has been replaced by **Develop a new optical pathlength model**.

<u>Task 2. Develop a new optical pathlength model</u> and **<u>Task 3. Apply random walk model to test model approaches</u>**

In this section, we will describe work performed in both tasks together for convenience. First, we briefly discuss the random walk model, since it is relevant in the discussion on both the development of the new model (Task 2) and in testing it (Task 3). Some model parameter definitions are shown in **Figure 1**. The scattering medium is an infinite slab with thickness *D.* Photons are scattered randomly multiple times and travel a total (integrated) pathlength within the medium of $L = \sum l_i$. Incoming photons are considered to be traveling as a pencil ray, as shown, whereas outgoing photons in all directions are collected.

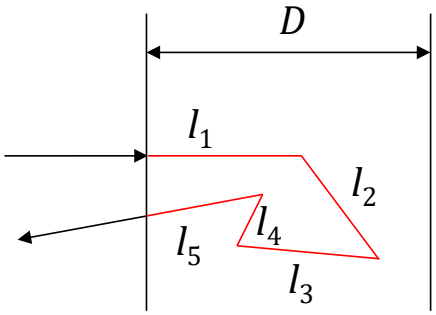

Figure 1. Schematic of multiple scatter events inside a TBC

Two random walk simulation codes were adapted and improved upon, one written in Labview and one in C++. In particular, the effects of integrated path-length needed to be incorporated in the simulation code, and tested. The validity of the two codes was tested in several ways, including the predictions of total transmission and reflection. The two codes were also compared with each other, in order to check consistency. For instance, **Figure 2** shows two integrated pathlength distributions computed with both models, using μ_s = 200 mm^{-1}.

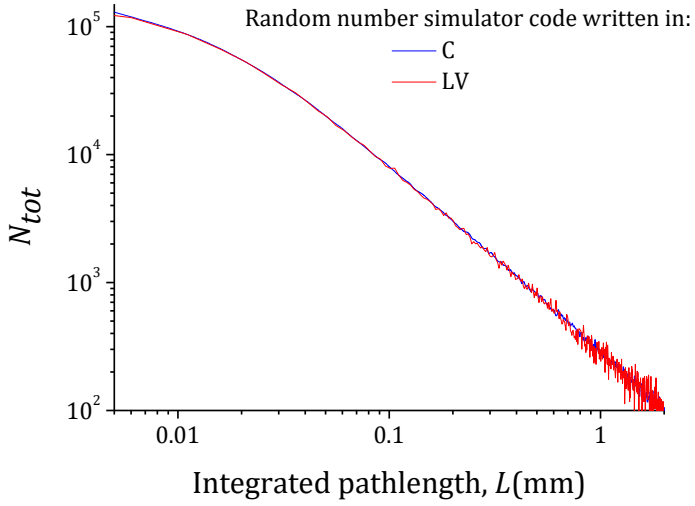

Figure 2. Comparison of pathlength distributions, as computed by two random number simulation codes developed for this project.

Ideal case: infinitely thick slab with scatter only

First, we look only at scattering process (i.e., absorption is set to zero), and furthermore neglect reflections at the interface. All diffusely reflected photons are considered, i.e. the collection optics are assumed to be irrelevant.

The first questions that arises, is what defines an infinite slab thickness, and what does the simulated signal look like in such a case. For that purpose, scatter coefficient (μ_s) and layer thickness (D) was varied in a set of simulations, of which **Figure 3** shows an example. It can be seen that the difference in D manifests itself only in the tail pathlength distribution. For instance, the simulated curves for (D=0.3 mm, μ_s=20 mm^{-1}) and (D=0.6 mm, μ_s=20 mm^{-1}) are overlapping up till approximately L = 0.1 mm, then diverge at higher values. The same is the case for the lines for (D=0.3, μ_s=40) and (D=0.6, μ_s=40), where the divergence occurs at slightly higher values of approximately L = 0.2 mm. This can be understood to be the result of the photons on average traveling a longer pathlength in a thicker medium , whereas for short integrated pathlengths the layer thickness is irrelevant.

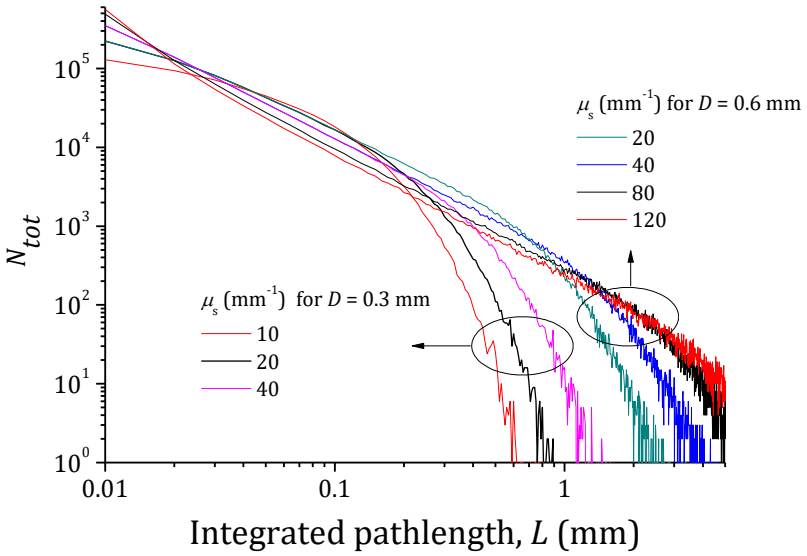

Figure 3. Effect of scatter coefficient and layer thickness on the heterodyne efficiency

Another set of integrated pathlength distribution simulations is shown in **Figure 4**, where the slab thickness D was varied in steps of factor 2 while the scatter coefficient μ_s= 200 mm^{-1}. Photons that reach the boundary were allowed to escape at the other end. Again, the effect of D on the pathlength distributions shows up in the tail of L, while for small values the curves overlap.

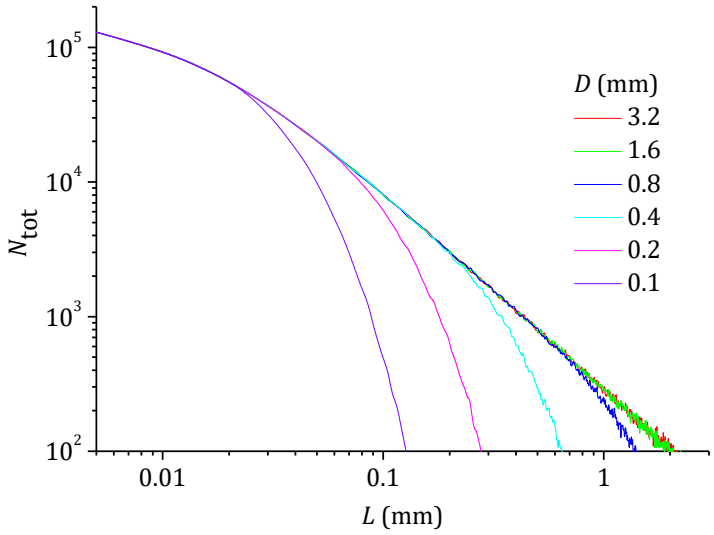

Figure 4. Integrated pathlength distributions for different values of slab thickness D

On the other hand, the difference in μ_s values manifests itself predominantly in the lower values for for L in the pathlength distribution, as is shown in **Figure 5**.

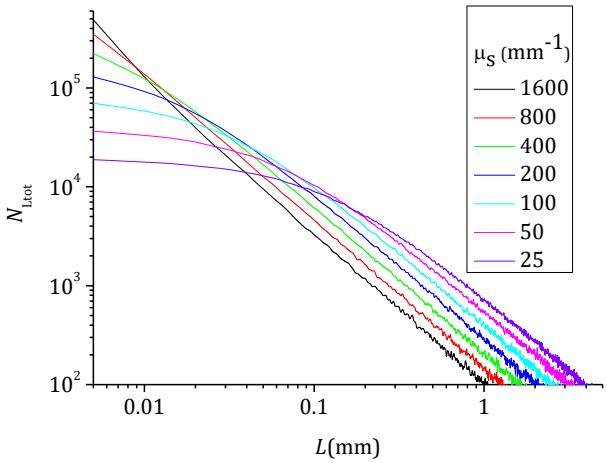

Figure 5. Integrated pathlength distributions as a function of scatter coefficient μ_s.

Thus, an infinitely thick coating exhibits a near straight line in the tail on a log-log plot, which indicates a power-law functionality. From these simulations, a condition for what defines an infinitely thick coating is therefore approximately $D \times \mu_s > 100$. The slope of the tail in the log-log plot is not affected by μ_s, only the low L value end of the pathlength distribution.

New optical pathlength distribution model

In this section, the basics of a new analytical model derived as part of the AFOSR project will be discussed. In parallel, OCT model work has also been undertaken at MetroLaser, Inc. (Irvine, California), under a USAF SBIR contract. In brief, the approach taken by MetroLaser is as follows. It was found that the OCT signal may be approximated by (and fit with) a power law function with form

$$A(L) \propto \left(1 + \frac{L}{L_s}\right)^{-n}, \tag{3}$$

where L_s is a characteristic length scaling factor and n expresses the degree of non-exponentiality and is considered to relate to the number of scatter events contributing to the signal. This decaying signal, in fact any decaying signal, may be defined as a sum of exponential components. In the continuous case, this is defined by the Laplace transform

$$A(L) = \int_0^\infty D(x) \exp\left(-\frac{L}{x}\right) dx, \tag{4}$$

Where $D(x)$ is the amplitude distribution function (or probability density function) for the various values of some characteristic pathlength x. When performing an inverse Laplace transform on this function, it was demonstrated by MetroLaser scientists that this results in a Poisson-like function

$$D(x) \propto \left(\frac{L_s}{x}\right)^{n-1} \exp\left(-\frac{L_s}{x}\right), \tag{5}$$

which may be used to correlate the signal with scatter coefficients of the medium.

From the point of view of signal processing, this approach is robust since the inverse Laplace

Transform is performed on a noiseless dataset, i.e., the fit with Eq. (3). That the kernel is a Poisson distribution appears in accordance with diffusion of light through a scattering medium, although the physical meaning of the exponent *n* is not entirely clear yet.

As mentioned above, the purpose of the work discussed in the present report is to likewise provide further theoretical underpinning of OCT measurements. The approach is to derive equations from first principles and compare the theoretical results with OCT measurements and numerical simulations. It is therefore of interest as well how the resulting theory compares with the above approach. In addition, OCT measurements at MetroLaser as a function of concentration [C] of scatterers indicate that the peaks of the distribution functions scale by $[C]^{-1/3}$, apparently violating Beer's law for optical transmission, while the random walk simulations predict a scaling with $[C]^{-1}$, in accordance with Beer's law. One way to find out how this difference may arise is to derive a theoretical framework and test various aspects of it with random walk models. Finally, the theoretical framework should allow us to evaluate under what conditions certain approximations are valid.

In deriving an analytical set of equations for the integrated pathlength, the approach taken in the present work was to define the problem in terms of probability distribution functions for the number of photons that travel a total pathlength L through a homogenously scattering medium with scatter coefficient μ_s following n scatter events. For instance, one can evaluate the first passage problem, i.e., evaluate the number of steps required to escape once the particle has entered the medium. The problem can be sub-divided into deriving probability functions for the number of photons that travel a distance L while undergoing n = 1, 2, 3, … scatter events. The summation of these probability functions should correspond to the OCT signal beam; i.e.

$$P_{total}(L) = P_1(L) + P_2(L) + \cdots = \sum_n P_n(L). \qquad (6)$$

It was found, by simulation, that the integrated individual terms over the path-length, i.e.,

$$P_n = \int P_n(L)dL\,. \qquad (7)$$

were independent of scatter cross-section μ_s, as shown in **Figure 6**. If true, this somewhat surprising result should also follow from deriving the explicit equations for $P_n(L)$. The values for n up to 10 are shown in the table to the right.

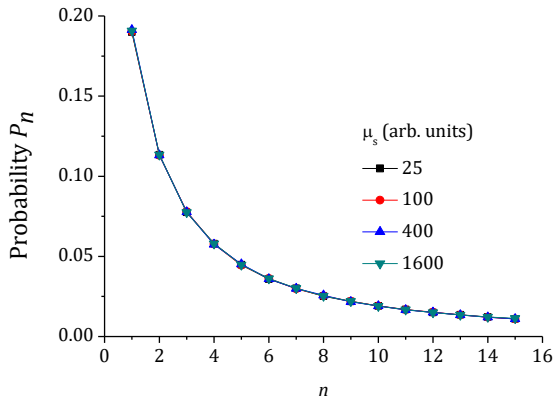

n	P_n
1	0.182
2	0.109
3	0.074
4	0.055
5	0.043
6	0.035
7	0.029
8	0.024
9	0.021
10	0.018

Figure 6. Probabilities P_n, from random number simulations.

In the following paragraphs, the derivation of these terms $P_n(L)$ will be discussed, starting with a derivation of the probability distribution function $P_1(L)$ and hence P_1.

$P_1(L)$ derivation

Consider the following geometrical arrangement, see **Figure 7**, whereby a collinear low coherence beam (shown as a red arrow) is considered to be incident onto the sample at normal incidence to the surface (shown as a circle).

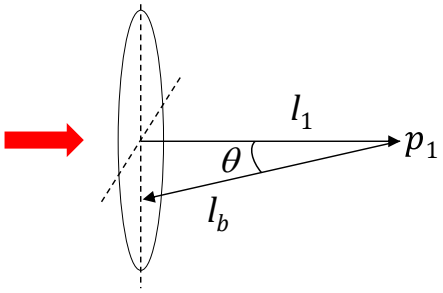

Figure 7. Optical geometry of one particular n = 1 scatter event.

The photons travel into the sample along the same direction, and scatter at some position p_1 along this line, at a distance l_1 from the boundary. The location p_1 is not a fixed position: the probability density function of the number of photons scattered at a position p_1 is defined by the exponential function

$$P_{p1}(l_1) = \mu_s \exp(-\mu_s l_1)\,. \tag{8}$$

Upon random scattering at location p_1, the photon travels in some arbitrary direction. Suppose the photon travels in the direction indicated by the arrow in **Figure 7**, is reach the boundary and escapes, and hence is scattered only once. The distance to the boundary is defined as l_b, such that the total distance that the photon has traveled is $L = l_1 + l_b$. Then, the probability distribution of total distance travelled (L) for the case of singly scattered photons, $P_1(L)$, may be defined as the integral product

$$P_1(L) = \int_{l_1=0}^{L/2} P_{esc}(l_b = L - l_1) P_{p1}(l_1) dl_1\,, \tag{9}$$

where $P_{esc}(l_b = L - l_1)$ is the escape probability for a photon traveling a distance l_b from the scatter location p_1 to the boundary, i.e., under the condition that it has traveled a path with total length L.

The following equation was derived for the escape probability as a function of distance d_b to the boundary:

$$P_{esc}(d_b) = \frac{1}{\pi} \int_0^{\frac{\pi}{2}} \exp\left(-\frac{\mu_s d_b}{\cos\theta}\right) d\theta. \tag{10}$$

In the above example if single scattering photons, d_b is simply equal to l_1. A closed form for the above integral may be obtained, but is not very compact and hence not shown here for brevity. Also, note that the integral has a singularity for $\theta = \frac{\pi}{2}$, nevertheless $P_{esc}(d_b)$ goes to zero as θ goes to $\frac{\pi}{2}$. The analytical solution of Eq. (10) and random number simulation results are compared in **Figure 8**.

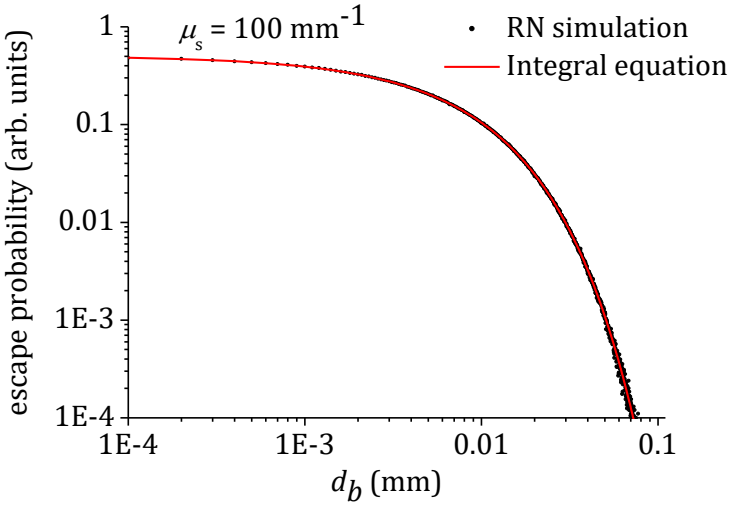

Figure 8. Escape probability $P_{esc}(d_b)$, computed with random number simulations and with Eq. (10).

When combining Eqs. (8)-(10), one can derive the following equation for $P_1(L)$:

$$P_1(L) = \left(\frac{1}{2} - \frac{1}{\pi}\right)\mu_s \exp(-\mu_s L)\,. \tag{11}$$

The total number of photons that are scattered only once can thus be found to be

$$P_1 = \int P_1(L)dL = \left(\frac{1}{2} - \frac{1}{\pi}\right) \sim 0.182\,. \tag{12}$$

It is thus found that P_1 is a constant and does not depend on the scatter coefficient. The value of 0.18 was verified with simulations, shown in the table in **Figure 6**.

higher order $P_n(L)$ terms

The first step in the derivation of the higher order terms is to define the probabilities of traveling a total distance L while undergoing 2, 3, etc. scatter events. This probability can be defined as the integral over three probabilities: the probability of scatter at location p_1, the probability of scatter at p_2 and the escape probability from p_2 under the condition that $L = l_1 + l_2 + l_b$:

$$P_2(L) = \int\int P_{p1}(l_1)P_{p2}(l_2)P_{esc}(d_b)dp_1 dp_2\,. \tag{13}$$

The geometrical arrangement of one such n = 2 scatter event is shown in **Figure 9**.

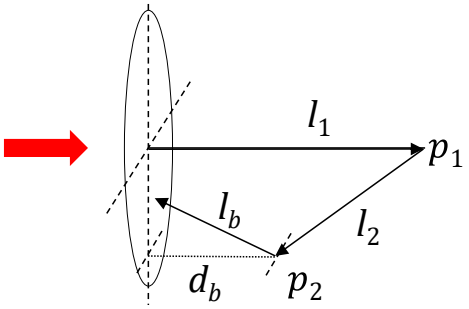

Figure 9. Optical geometry of one particular n = 2 scatter event.

The solution to Eq. (13) is non-trivial, and full derivation will be presented at a later stage. Part of the solution is the definition of the probability of traveling a distance d_z along the z-axis following an isotropic scatter event, which was derived to be described by:

$$P_{dz}(d_z) = \frac{\mu_s}{2\pi}\int_0^{\frac{\pi}{2}} \frac{\exp(-\mu_s d_z \sin^{-1}\theta)}{\sin\theta} d\theta \tag{14}$$

The following graph shows the probability density function of $P_{dz}(d_z)$ together with a random number simulation of the same process:

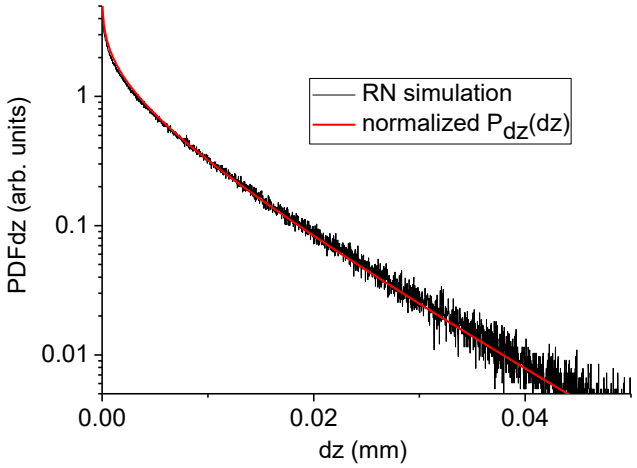

Figure 10. probability of traveling a distance *dz* following a scatter event: random number simulation versus Eq. (14).

Working model of higher order $P_n(L)$ terms

While explicit forms of $P_n(L)$ are preferred, the following semi-theoretical approach was used to derive a working model.

In general, the probability of undergoing n scatter events over a distance L, with an average number of events $\lambda = \mu_s L$, is given by the Poisson distribution

$$P_s(n, L) = \frac{(\mu_s L)^n \exp(-\mu_s L)}{n!} \tag{15}$$

The random walk simulation was used to test how this distribution comes into play in the overall pathlength distribution signal $P_{total}(L)$. It became evident that instead of the above equation, a slightly different version was fully describing the number of photons that travel a distance z, let's call it F :

$$F_n(L) = \text{constant} \times \frac{(\mu_s L)^{n-1} \exp(-\mu_s L)}{(n-1)!}, \tag{16}$$

where the constant depends on n. Specifically, the function that was used to fit the histogram curves from random number simulations was

$$F_n(L) = a_n \mu_s \frac{(\mu_s L)^{n-1} \exp(-\mu_s L)}{(n-1)!}, \tag{17}$$

where a_n are scaling factors. **Figure 11** shows four histograms for different values of n, using μ_s=100 mm^{-1} (the actual value of $\mu_s$is not relevant), together with the fitting function of Eq. (17). Note that n, L, and μ_s in fitting function $F_n(L)$ are constants; only the scaling factor a_n is used as a fitting variable.

Two observations are made; firstly, for n = 1 Eq. (17) reduces to $F_1(L) = a_n\mu_s\exp(-\mu_s L)$ and the fitting value a_1 is found to be 0.18, i.e. close to the value of $\left(\frac{1}{2} - \frac{1}{\pi}\right)$ of Eq. (12).

Secondly, the other fitting parameters a_3, a_5 and a_{10} as shown in **Figure 11** are very close to the values P_3, P_5 and P_{10} as shown in the table of **Figure 6**. Observation of other results revealed that in general a_n has approximately the same value as P_n. One can see that Eq. (17) divided by a_n are probability functions with unity total probability, hence a_n are simply the normalization constants that determine the integrated values of the probability density functions.

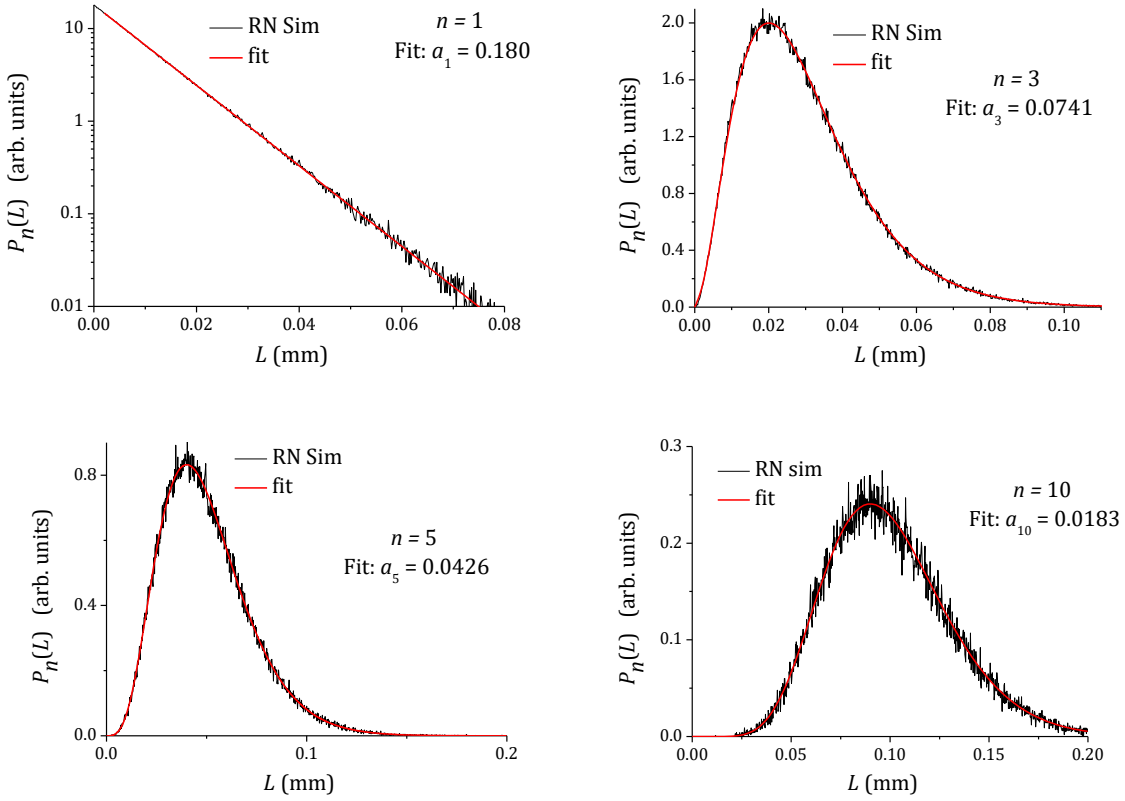

Figure 11. Probability distribution functions $P_n(L)$ from random number simulation and using fitting function Eq. (17), for n = 1, 3, 5 and 10. In all cases, μ_s=100 mm^{-1}

Thus one can assume that the fitting function Eq. (17) serves as a good working model for the OCT signal modeled by the random number simulation code. The extent to which this model is suitable for real OCT signals will be evaluated subsequently. So the signal beam photon count in this idealized case (since the optical geometry is not taken into account, and several other idealizations are in effect) can be approximated by rewriting the terms of Eq. (17) and summing over n:

$$\text{Signal} \propto S(L) = \sum_{n=1}^{\infty} F_n(L) = \sum_{n=1}^{\infty} \frac{a_n {\mu_s}^n}{(n-1)!} L^{n-1}\exp(-\mu_s L) \qquad (18)$$

The upper limit in the summation is taken to be infinite, however in reality there is likely an upper limit in the number of scatter events that can be measured. However, the decrease in coefficients a_n already take care of this reduced sensitivity of the measurement to higher numbers of scatter events. Since the exponential term does not contain n, and to start the summation with n = 0, we can rewrite Eq. (18) as

$$S(L) = \mu_s \exp(-\mu_s L) \sum_{n=0}^{\infty} \frac{a_{n+1}}{n!} (\mu_s L)^n \qquad (19)$$

An example of a comparison between Eq. (19) and the full histogram as computed with RN simulation is shown in **Figure 12**, which was obtained for μ_s=100 mm^{-1}. Instead of an infinite number of terms, the graph shows the summation of Eq. (19) over terms with n = 0 – 130. As might be expected, the power series of Eq. (19) was found to describe the simulated signal histogram well, for a given range of L: the smaller the number of terms (i.e., for smaller upper n), the shorter the range of L over which Eq. (19) compares well with the RN simulation. The range of L which is well described by Eq. (19) is roughly n_{upper}/μ_s.

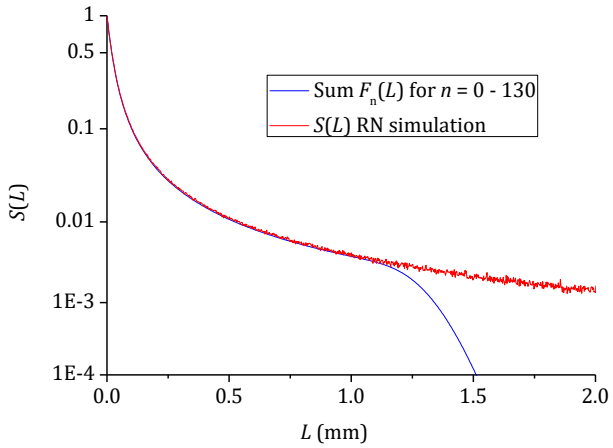

Figure 12. Signal function as obtained from RN calculations and computed with Eq. (19) for a finite range of terms, for n = 0 to 130, for μ_s=100 mm^{-1}.

It is noted that the signal function has the form of a *Poisson Generating Function*, i.e.

$$S(L) = PG(a_n; x) = \sum_{n=0}^{\infty} \frac{a_n}{n!} e^{-x} x^n \qquad (20)$$

The use of a_{n+1} instead of a_n in Eq. (19) is arbitrary and hence insignificant.

Relation with MetroLaser model

In this section, the goal is to see how the above derivation relates to the MetroLaser (ML) model.

The basic principles of the ML model is that the OCT signal of a randomly (diffuse) scattering medium appears to fit well to a power law function of the form

$$F_{PL}(L) = \frac{a}{(1+bL)^c} \qquad (21)$$

In turn, by means of the inverse Laplace Transform this power law function can be converted to a Poisson-like kernel function, from which a correlation with scatter coefficient may be obtained.

First, it is worth checking how well the simulated signal is fit with Eq. (21). This can be seen in **Figure 13**. As can be seen, Eq. (21) doesn't fit the simulated data entirely well. The fit values obtained were a = 1.01; b = 24.0 and c = 1.82. In order to make a better fit, a baseline value can be added, as is done in the ML approach. However, the physical interpretation of this baseline value is not clear in the present model, since it predicts that the signal decreases to zero for large enough L.

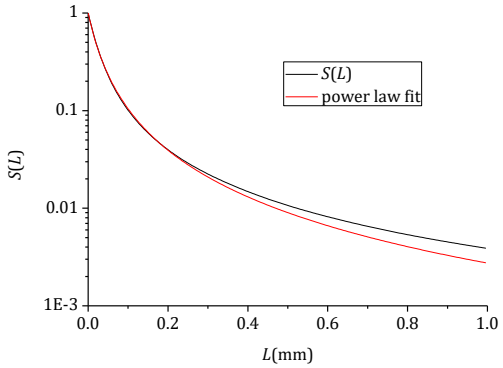

Figure 13. Signal function $S(L)$ and a fit with power law function from Eq. (21), for μ_s=100 mm^{-1}.

Next, instead of starting with a signal (either simulated or real) and trying to extract a kernel function via the inverse Laplace Transform, it is of interest to see how the signal function Eq. (19) itself can be expressed as a (direct) Laplace Transform, and if so, to what function this transformation leads.

In general, any power series

$$\sum_{n=0}^{\infty} b_n x^n \tag{22}$$

can be converted to an integral (i.e., continuous) form of the Laplace Transform by making three substitutions: (1) exchange integer n for a continuous parameter t; (2) defining $-s = \ln x$; and (3) multiplying b_n with the Dirac delta function $\delta(t-n)$. In that case, one gets

$$\sum_{n=0}^{\infty} b_n x^n = \int_0^{\infty} b(t)\exp(-st)dt = \mathcal{L}\{b(t)\}. \tag{23}$$

Thus, we see that the signal function $S(L)$ can be written as a Laplace Transform of a function that contains the constants a_{n+1}:

$$S(L) = \mathcal{L}\{a(t)\} \tag{24}$$

where

$$a(t) = \mu_s \frac{a_{n+1}}{n!} \exp(-\mu_s L)\, \delta(t-n) \tag{25}$$

Thus, we see that in the current approach, the Poisson generating signal function Eq. (19) can in principle be converted into a Laplace transform. Although numerical values of the coefficients a_n are known, it will be of value to define them analytically, which is being investigated. Whether this leads exactly to a power law function of the form of Eq. (21) remains to be seen. Considering that Eq. (21) does not fit simulated data perfectly well unless a baseline is added, the current approach may likely lead to a different signal function.

CHANGES IN SCHEDULE

A no-cost extension of will be requested for this project, with a new project end date of 30 June 2017.

WORK PLAN FOR NEXT REPORTING PERIOD

In the next reporting period, the remaining tasks of this project will be conducted, including

1. Finalize the new analytical model by incorporating the effect of absorption and interface reflections on the integrated pathlength distribution
2. Evaluate the new model with random walk simulations
3. Analyse experimental data with the new model
4. Submit the final report.

PERSONNEL SUPPORTED

Personnel working on this project was B. Heeg, Ph.D.

COST SUMMARY

As of this date, 280 hours have been billed to the project, leaving a total of 120 hours to bill to the project.

REFERENCES

1] G. Popescu and A. Dogariu, "Optical path-length spectroscopy of wave propagation in random media", *Opt. Lett.* 24, 442 (1999).

2] J.I. Eldridge, C.M. Spuckler and J.R. Markham, "Determination of Scattering and Absorption Coefficients for Plasma-Sprayed Yttria-Stabilized Zirconia Thermal Barrier Coatings at Elevated Temperatures", *J. Am. Ceram. Soc.* 92, 2276 (2009).

3] L. Wang, J.I. Eldridge and S.M. Guo, "Comparison of different models for the determination of the absorption and scattering coefficients of thermal barrier coatings", *Acta Materialia* 64, 402 (2014).

4] A.M. Limarga and D.R. Clarke, "Characterization of Electron Beam Physical Vapor-Deposited Thermal Barrier Coatings Using Diffuse Optical Reflectance", *Int. J. Appl. Ceram. Technol.* 6, 400 (2009).

5] L. Thrane, M.H. Frosz, D. Levitz, T.M. Jørgensen, C.B. Andersen, P.R. Hansen, J. Valanciunaite, J. Swartling, S. Andersson-Engels, A. Tycho, H.T. Yura, P. Andersen, "Extraction of tissue optical properties from optical coherence tomography images for diagnostic purposes" SPIE Vol. 5771, 139 (2005).

6] M.S. Patterson, B. Chance and B.C. Wilson, "Time resolved reflectance and transmittance for the non-invasive measurement of tissue optical properties", *Appl. Opt.* 28, 2331 (1989).